J|A|C|S
ARTICLES
Published on Web 03/29/2007

Molecular Electrodes at the Exposed Edge of Metal/Insulator/Metal Trilayer Structures

Pawan Tyagi,[†] Dongfeng Li,[‡] Stephen M. Holmes,[‡] and Bruce J. Hinds*[,†,‡]

Contribution from the Department of Chemical and Materials Engineering and Center for Nanoscale Science and Engineering, University of Kentucky, Lexington, Kentucky 40506-0046, and Department of Chemistry, University of Kentucky, Lexington, Kentucky 40506-0055

Received August 9, 2006; E-mail: bjhinds@engr.uky.edu

Abstract: Producing reliable electrical contacts of molecular dimensions has been a critical challenge in the field of molecule-based electronics. Conventional thin film deposition and photolithography techniques have been utilized to construct novel nanometer-sized electrodes on the exposed vertical plane on the edge of a thin film multilayer structure (metal/insulator/metal). Via thiol surface attachment to metal leads, an array of paramagnetic, cyanide-bridged octametal complexes, $[(pzTp)Fe^{III}(CN)_3]_4[Ni^{II}(L)]_4[O_3SCF_3]_4$ (**1**) [(pzTp) = tetra(pyrazol-1-yl)borate; L = 1-S(acetyl)tris(pyrazolyl)decane], were covalently linked onto the electrodes forming a dominant conduction pathway. A series of molecule-based devices were fabricated using Ni, NiFe, Ta, and Au as metal electrodes separated by insulating Al_2O_3 spacers, followed by treatment with **1**. A series of control experiments were also performed to demonstrate that the conduction path was through tethered metal clusters. The molecular current was analyzed via the Simmons tunnel model, and calculations are consistent with electron tunneling through the alkane ethers to the central metal core. With a $Ni/Al_2O_3/Au$ molecular electrode, the tether binding was found to be reversible to the top Au layer, allowing for a new class of chemical detection based on the steric bulk of coordinating analytes to disconnect the molecular current path. Simple and economical photolithography/liftoff/self-assembly fabrication techniques afford robust molecular junctions with high reproducibility (>90%) and long operational lifetimes (>1 year).

Introduction

An ultimate goal of electronics miniaturization is to have discrete molecules act as logic or switching elements. An advantage to this approach is that the molecules can be synthesized reproducibly at the angstrom scale with well-defined electronic states tuned through chemical functionality. Electrical transport through molecules has been investigated via a variety of theoretical[1] and experimental methods, with promising observations such as negative differential resistance,[2] spin-state dependent conduction[3,4] and stable memory based on conformational shifts being demonstrated recently.[5] To date, no single fabrication approach has allowed for the facile integration of molecules into circuit architectures. For molecule-based electronics to become a technological reality, electrode architectures must be engineered with nanometer-scale dimensions and allow for the incorporation of molecules that can be synthesized and tuned with angstrom-level precision and well-defined electronic or spin states.

One of the major challenges in the field has been to reliably integrate molecules into circuit architectures, where mass produced electrodes with gaps at the nanometer scale and angstrom precision are needed. In particular, it has been difficult to reliably make electrodes where electron conduction travels along the length of a molecule. Initial studies of molecular currents through isolated molecules utilized 1,4-benzenedithiols inserted into gold break junctions, prepared via mechanical or electromigration tehniques,[6] where atomically sharp points terminate each electrode, separated by nanometer-sized gaps. While this is an experimentally attainable process, it is exceedingly difficult to control the dimensions of the gap between electrodes. This requires tedious analysis of the prepared break junction devices, to ensure that conduction through the molecules dominates rather than electron hopping via nanometer-scale metallic islands (Coulombic blockade).[7] A second approach for contacting molecules lengthwise utilizes densely packed arrays of molecules on metallic surfaces, followed by careful deposition of metal films onto the self-assembled monolayer (SAM) array. Unfortunately this approach suffers from electrical shorts through defect areas, which can be minimized through the use of small contact areas located in

[†] Department of Chemical and Materials Engineering and Center for Nanoscale Science and Engineering.
[‡] Department of Chemistry.

(1) Aviram, A.; Ratner, M. A. *Chem. Phys. Lett.* **1974**, *29*, 277−283.
(2) Chen, J.; Reed, M. A.; Rawlett, A. M.; Tour, J. M. *Science* **1999**, *286*, 1550−1552.
(3) Liang, W. J.; Shores, M. P.; Bockrath, M.; Long, J. R.; Park, H. *Nature* **2002**, *417*, 725−729.
(4) Park, J.; Pasupathy, A. N.; Goldsmith, J. I.; Chang, C.; Yaish, Y.; Petta, J. R.; Rinkoski, M.; Sethna, J. P.; Abruna, H. D.; McEuen, P. L.; Ralph, D. C. *Nature* **2002**, *417*, 722−725.
(5) Collier, C. P.; Wong, E. W.; Belohradsky, M.; Raymo, F. M.; Stoddart, J. F.; Kuekes, P. J.; Williams, R. S.; Heath, J. R. *Science* **1999**, *285*, 391−394.
(6) Reed, M. A.; Zhou, C.; Muller, C. J.; Burgin, T. P.; Tour, J. M. *Science* **1997**, *278*, 252−254.
(7) Yu, L. H.; Natelson, D. *Nano Lett.* **2004**, *4*, 79−83.

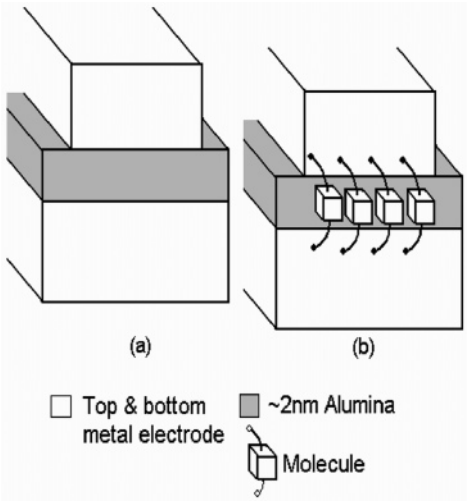

Figure 1. **(a)** Schematic of multilayer electrode geometry with nanometer-scale insulator spacing between metal electrodes **(b)** Schematic of molecules bridging across insulator to provide molecular current path. Conducting molecules are at the pattern edge surface, and those molecules that do not span the insulator are not electrically active.

nanopores,[8] micropatterns, or areas under gold nanocrystals.[9] While these structures are useful for studying molecular conduction processes, they do not allow for external gating nor possess exposed regions for chemical sensing.

A third promising approach utilizes molecular wires that require only two metallic terminals and whose logic function is determined by the applied bias and location of a charged rotaxane molecule along the length of a conductive chain. To minimize electrical shorting of the electrical terminals, incorporation of the rotoxane assemblies under the small area (20 nm $\times$ 20 nm) of crossed metallic nanowires allows for each junction to be addressed and logic architectures to be formed.[10] However, a significant challenge in this approach is the reliable alignment of nanowires into multimillion node arrays for very large-scale integration (VLSI) applications. A technique that utilizes established scaleable processes, such as photolithography and thin film deposition to produce electrodes with gap lengths of molecular dimensions, is critical for the advancement of molecular electronic applications.

Conventional thin film deposition processes can control film thickness with angstrom-level precision; however, utilizing this planar dimension offered integration challenges. On the perpendicular surface of the patterned, multilayer, thin film structure edge, there are by necessity parallel lines of material that have widths corresponding to the thickness of deposited films. For example, selective material etching followed by transfer to imprint lithography masks allows for transfer of the parallel lines with nanometer-scale pitch.[11] The principle of film thickness for critical dimensional control has also been applied to the formation of vertical transistors with gate lengths corresponding to thicknesses of the thin films.[12] This film thickness approach has been utilized to construct electrode gaps after selective chemical etching of a thin barrier layer, as in the case of thin sections along template-grown nanowires[13] or on patterned $Si/SiO_2/Si$ structures.[14] In the former case, the smallest gap attained was 5 nm which would require relatively long molecules. Integration of these wires without adjustment (mechanical bending of the wire) of the gap width into large-scale architecture remains a significant challenge. However, $Si/SiO_2/Si$ gap structures are easily integrated into circuit designs, but for films that are ca. $\leq$5 nm thick, significant 1/frequency noise after the etching is found.[14,15] Moreover, chemical functionalization of Si surfaces without an intermediate oxide layer also presents great difficulty. Clearly, an alternate scaleable approach that can generate electrode gap lengths on the order of large conductive molecules (ca. 2 nm), that allows for a range of metallic contacts, and variety of surface chemistries is required for reliable molecular electronics.

We have developed an alternative strategy for preparing reliable molecular electrodes as diagrammed in Figure 1. A metal/insulator/metal multilayer structure was grown, and there was a narrow "line" of insulator material on the perpendicular plane at the pattern edge. This formed a "gap" where surface molecules could bridge across the insulator to become the primary current path. Surface molecules that did not bridge across the insulator layer did not contribute to the current between the leads. Critical to the feasibility of this approach was to have the "background" current of the bare electrode (without molecules) much less than the case after molecular bridging. In general the background current is primarily due to tunneling current through the insulator in the relatively large planar area of the electrode (5 μm $\times$ 5 μm). At insulator thicknesses less than 2 nm, this tunnel current can be dominant over a monolayer of surface molecules at the pattern edge. The process was experimentally optimized by the deposition of uniform and nearly defect-free insulating oxides. A molecule had to be designed which was large enough to span an experimentally reasonable tunnel barrier thickness and that was sufficiently conducting, readily soluble, and had a well-defined rigid structure. Herein we present a fabrication methodology to prepare a multilayer edge molecular electrode (MEME) geometry by two techniques and offer experimental evidence showing that current conduction is dominated by surface molecules spanning the insulator gap. A sharp exposed edge of multilayer, a critical step in MEME fabrication, was produced by using both ion milling and photolithography-liftoff processes. Although both processes resulted in similar transport properties, the photolithography approach was adopted due to fabrication ease and high device yield ($\sim$90%). Control experiments included the reversible binding of a conductive molecule across the insulator gap with consistent changes in current. Phenomenological modeling of electron transport was consistent with tunneling through alkane tethers to and from the core of a metal-cluster molecule.

(8) Mbindyo, J. K. N.; Mallouk, T. E.; Mattzela, J. B.; Kratochvilova, I.; Razavi, B.; Jackson, T. N.; Mayer, T. S. *J. Am. Chem. Soc.* **2002**, *124*, 4020−4026.
(9) Gittins, D. I.; Bethell, D.; Schiffrin, D. J.; Nichols, R. J. *Nature* **2000**, *408*, 67−69.
(10) Beckman, R.; Johnston-Halperin, E.; Luo, Y.; Green, J. E.; Heath, J. R. *Science* **2005**, *310*, 465−468.
(11) Melosh, N. A.; Boukai, A.; Diana, F.; Gerardot, B.; Badolato, A.; Petroff, P. M.; Heath, J. R. *Science* **2003**, *300*, 112−115.
(12) Gossner, H.; Wittmann, F.; Eisele, I.; Grabolla, T.; Behammer, D. *Electron. Lett.* **1995**, *31*, 1394−1396.
(13) Qin, L. D.; Park, S.; Huang, L.; Mirkin, C. A. *Science* **2005**, *309*, 113−115.
(14) Berg, J.; Lundgren, P.; Enoksson, P.; Bengtsson, S. *Appl. Phys. Lett.* **2005**, *87*, 22.
(15) Dirk, S. M.; Howell, S. W.; Zmuda, S.; Childs, K.; Blain, M.; Simonson, R. J.; Wheeler, D. R. *Nanotechnology* **2005**, *16*, 1983−1985.

Physical Methods

Throughout this work, a thermally grown 100-nm silicon oxide (SiO_2) isolation layer was used as the substrate. Prior to every photolithography step, substrates were first sequentially cleaned with acetone (2 × 10 mL) , (2 × 10 mL) and in deionized (DI) water (2 × 10 mL), and then dried in flowing nitrogen. The pattern areas were defined by a conventional photolithography method using Shipley 1813 positive photoresist and a Karl Suss mask aligner. Photoresist thickness, exposure time, and developing steps were optimized to obtain a suitable edge profile. After the required film deposition steps, a gentle liftoff process was carried out with a Shipley 1165 resist remover for 2−4 h. The liftoff step was critical for the photolithography-liftoff produced MEME sample because success in exposing the side edge of a tunnel junction for molecule hosting depends upon liftoff efficacy. The metal films for multilayer, molecular electrode fabrication were sputtered using an AJA International Sputtering system. For all the depositions, base pressure was ~2×10^{-7} Torr. Top and bottom metal films of all the molecular electrodes were deposited at 2m Torr argon pressure and 150 W power with an RF sputtering gun. Gold (Au), nickel (Ni), cobalt (Co), nickel−iron (Ni:Fe::80:20) and tantalum (Ta) metals were sputter deposited as top and bottom metal films, respectively, of different multilayer tunnel junctions. Root-mean-square roughness measured by AFM for all the metal films was around ~0.2 nm. Deposition of the 2-nm thick alumina insulator, the most important step of molecular electrode fabrication scheme, was accomplished using a multistep process. To have a uniform coating of the insulator, aluminum (Al) metal was first deposited on top of the bottom metal electrode, since similar surface energies of metals result in good wetting without island growth. Al metal was deposited from a DC powered gun at 75 W power and 2 mTorr Ar pressure. The Al film (1 nm) was then subsequently plasma oxidized with 60 mTorr of 1:1 argon and oxygen gas mixture for 30 s at 20 W substrate bias in sputtering chamber. A second Al deposition (0.5 nm) followed by plasma oxidation was performed to give an optimal tunnel barrier quality for a ~2.0 nm thick insulating layer with a breakdown voltage ranging from 1.8 to 2.5 V. The typical tunnel junction area and contact resistance were ~10−25 μm^2 and ~1 MΩ, respectively, for all the MEME samples. Dimensions of cross junctions were chosen according to our photolithography resolution limit and were optimized to reduce shorting defects in the cross-junction area. Particularly intense experimental effort was required to optimize the conditions of deposition (power, pressure, and seed layer material) such that the metal surfaces had less than 0.2 nm rms smoothness as measured by tapping mode AFM (Digital Instruments Multimode). Another critical experimental optimization was to minimize compressive stress in the deposited films. This was because we observed that the stress release mechanism involves the formation of hillocks that short across the tunnel barrier, dramatically reducing the temporal and thermal stability of the device.

The exposed pattern edges were produced by two fabrication approaches. In the first approach, shown in Figure 2, Scheme A, ion beam milling (FISCHIONE 1010 ion mill) was employed to produce the edge, a well-established method to produce atomically sharp and exposed side edges of tunnel junctions.[16]

The ion-milled samples were cooled by liquid nitrogen during ion milling to minimize photoresist hardening; however, thermal stresses introduced tunnel junction instabilities and a short device life. To overcome the limitations of ion milling, a MEME fabrication scheme based on liftoff photolithography to define the pattern edge (Figure 2, Scheme B) was adopted. The scheme consists of (a) initial sputter deposition of metal onto an oxidized silicon surface in patterned window, followed by (b) photoresist window definition of cross-junction window, (c) sputter deposition of aluminum metal and subsequent plasma oxidation (O_2) with repeated cycles to give a ca. 2 nm thick alumina (Al_2O_3) film, (d) top contact metal sputter final deposition, and (e) liftoff removal of metal layer to leave exposed edge and three-dimensional perspective before (f) and after (g) molecular attachment. In this scheme, a key step is the deposition of ~2 nm insulator and top metal electrode in the positive photoresist window. The advantage of this method is that the planar dimension of the alumina barrier and top metal electrodes are controlled by the same photoresist boundaries. At the length scales involved in the normal direction (~3 nm) the photoresist is essentially atomically flat (0.2 nm rms for 50 nm × 50 nm area AFM scans), providing a sharp pattern. Scanning electron microscope (SEM) and AFM studies of a typical cross junction produced by scheme B are shown in Figure 3.

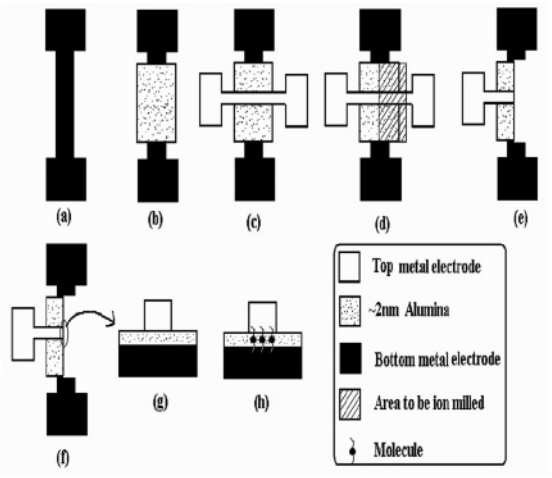

Scheme A

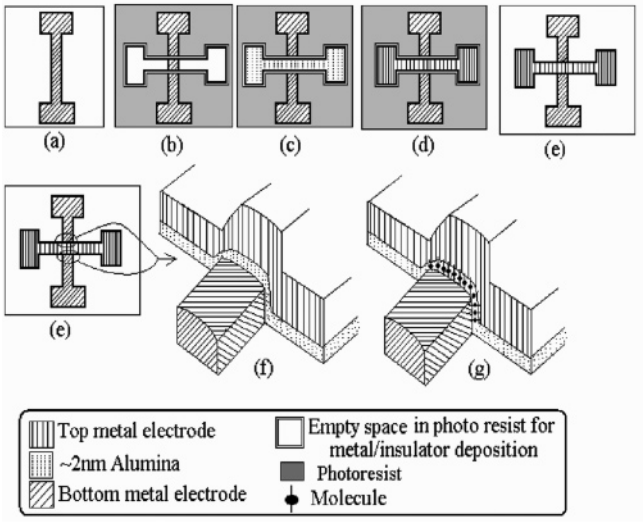

Scheme B

Figure 2. Multilayer edge molecular electrode (MEME) fabrication for (A) Ion-milling-based molecular electrodes: First a complete metal−insulator−metal tunnel junction is prepared by successive photolithography and liftoff steps in the shown regions (a−c). This is followed by ion milling in the specified shaded area of (d) to produce sharp exposed edge of MEME (e−g) and then molecule **1** is attached to the exposed edge (h). (B) Photolithography-pattern-based (MEME): Bottom metal electrode deposition (a) followed by the photoresist window for top insulator/electrode (b). Deposition of ~2 nm alumina (c) top metal electrode film deposition (d) followed by liftoff to produce sharp edge (e, f). Molecule attachment of **1** on the surface of exposed side completes molecular junction fabrication (g).

(16) Song, Y. S.; Park, S. J.; Kim, T. W.; Chung, C. W. *Electrochem. Solid State Lett.* **2004**, *7*, C64−C66.

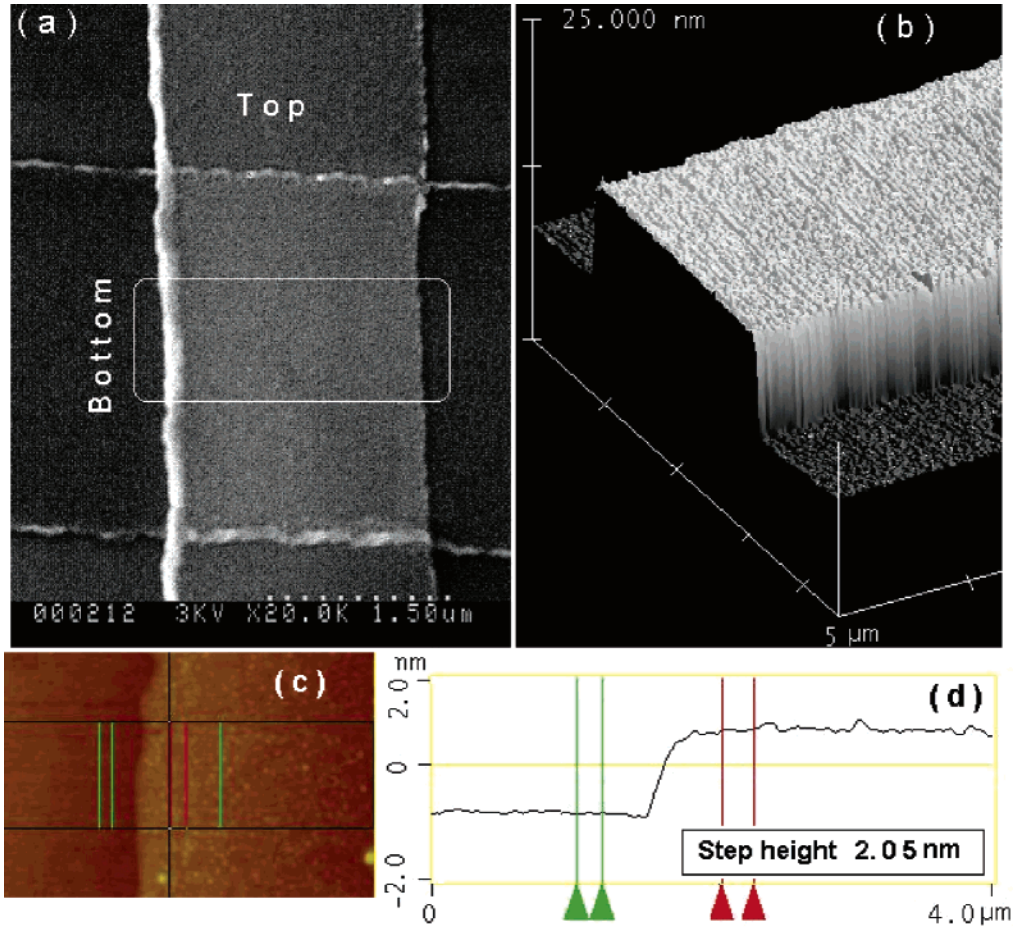

Figure 3. (a) SEM micrograph of a photolithography-liftoff-produced tunnel junction with exposed metal−insulator−metal side edges. (b) 3D view from AFM study of exposed side edge in the box of (a), 2-nm thick alumina deposited before top metal electrode is not resolved. (c) Topography and (d) step height measurement of alumina grown in a typical photoresist cavity is continuous and appears with exposed sides after clean liftoff.

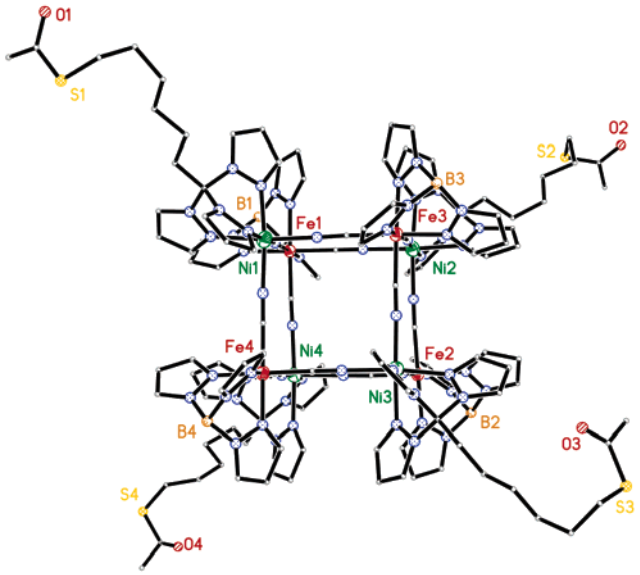

Figure 4. X-ray crystal structure of a structural analogue of **2** (figure adaped from ref 17). Cubic cluster consists of alternating Fe^{III} and Ni^{II} centers (corners) bridged by cyano groups (edges). All anions, H atoms, pendant pyrazoles, and disordered S(acetyl)hexyl- chains are removed for clarity. Note: 1-S(acetyl)tris(pyrazolyl)decane was used in electrode studies.

A molecule that can chemically link and bridge both electrodes has been developed by Holmes and co-workers.[17] To date only microcrystalline powders of **1**, $\{[(pzTp)Fe^{III}(CN)_3]_4[Ni^{II}(L)]_4\}_4[O_3SCF_3]_4\}$ (pzTp = tetra(pyrazol-1-yl)borate; L = 1-S(acetyl)tris(pyrazol-1-yl)decane), have been available, precluding X-ray structural studies; a structural analogue (**2**), where L = 1-S(acetyl)tris(pyrazol-1-yl)hexane, is illustrated in Figure 4.[17] In **2** the Fe^{III} and Ni^{II} centers reside in alternate corners of a slightly distorted box and are linked via cyanides (Figure 4). The cluster core contains coordinated tris(pyrazolyl)decyl- chains that are terminated with S(acetyl) groups at alternate corners (Ni^{II} centers) of the cubic cluster.[18] The S(acetyl) groups were chosen for several reasons: (1) there is ample literature precedence in self-assembled monolayer (SAM) formation, (2) acetyl protection prevents sulfur atom coordination to transition-metal centers during complex synthesis, (3) acetyl protection circumvents the use of air-sensitive thiols, and (4) acetyl groups are easily removed by electrochemical or chemical means. Electrochemical attachment of the clusters to the MEME electrodes via the thiolacetyl terminii[19,20] was accomplished via immersion of the electrodes in a dichloromethane solution of **1**, followed by alternating a ±100 mV bias between the two metal electrodes at a time interval of 0.01 s for 2 min. Subsequently, the assembled devices were rinsed with dichlromethane, 2-propanol, and deionized water and were dried under a nitrogen gas stream. Immersion of the MEMEs in a dichloromethane solution of **1** without performing the electrochemical step did not affect transport properties of exposed edge tunnel junctions.

(17) Li, D. F.; Parkin, S.; Wang, G. B.; Yee, G. T.; Clerac, R.; Wernsdorfer, W.; Holmes, S. M. *J. Am. Chem. Soc.* **2006**, *128*, 4214−4215.
(18) Li, D.; Clérac, R.; Parkin, S.; Wang, G.; Yee, G. T.; Holmes, S. M. *Inorg. Chem.* **2006**, *45*, 7569−7571.
(19) Maya, F.; Flatt, A. K.; Stewart, M. P.; Shen, D. E.; Tour, J. M. *Chem. Mater.* **2004**, *16*, 2987−2997.
(20) Inman, C. E.; Reed, S. M.; Hutchison, J. E. *Langmuir* **2004**, *20*, 9144−9150.

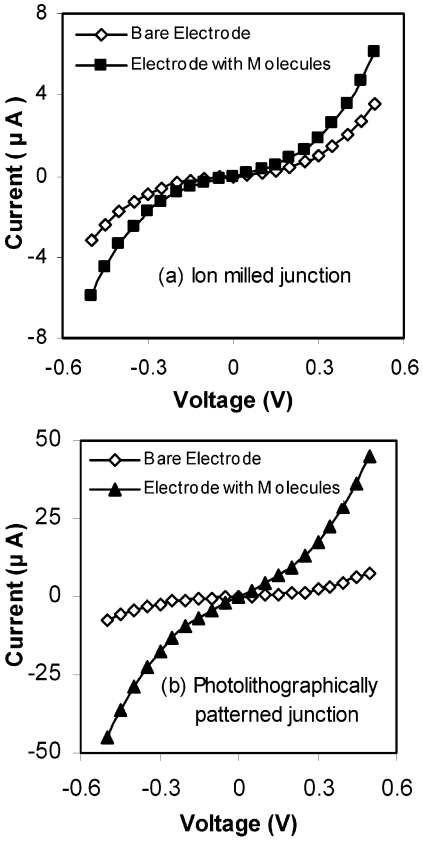

Figure 5. Current−voltage characteristics of multilayer edge molecular electrodes before (◇) and after (■ and ▲) molecular attachment for (a) ion-milled Co/NiFe/Al_2O_3/NiFe (Figure 2, Scheme A) and (b) photolithography defined Co/NiFe/Al_2O_3/NiFe electrodes (Figure 2, Scheme B).

Transport measurements of the tunnel junctions were obtained before and after attachment of molecules. The current was measured while the voltage was swept between ±100 mV for normal transport measurements, while a ±500mV range was chosen for determining the tunnel barrier properties; these voltage ranges are far below the breakdown voltage potentials (ca. 2 V) of the devices. Typically 3−5 measurements per each $I-V$ plot, using a 5 mV voltage and 0.5−1 s time steps were collected for each sample, to minimize possible scan-to-scan variation error.

Results and Discussions

Molecules on Ion-Milled Molecular Electrodes with Atomically Sharp Exposed Edges. To probe our hypothesis that the perpendicular plane of a tunnel junction at a pattern edge can be used for molecular electrode formation, we began with MEMEs prepared via ion-milling methods (Figure 2, Scheme A). For our comparative studies, film thicknesses (from bottom to top) were utilized: Si/SiO_2 (100 nm), Co (8 nm), NiFe (2 nm), Al_2O_3 (2 nm), and NiFe (10 nm).

The transport properties of ion-milled MEMEs both before and after attachment of **1** is shown in Figure 5a. A marked increase of 140% in current (current of ion-milled tunnel junction before and after molecule attachment at 100 mV was 1.35×10^{-7} and 3.07×10^{-7} A respectively) after attachment of molecules is observed, suggesting that current through the molecules exceeds the background tunnel current of the bare junction. Bare MEME tunnel samples did not show more than a 5% increase in current with electrical stress or exposure to neat solvents used in molecular attachment processes. Unfortunately, ion milling introduced significant thermal stresses and afforded samples that developed high current ohmic shorts after a few days.

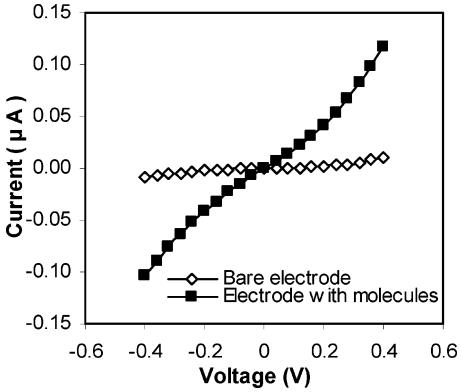

Figure 6. Current versus voltage behavior of Ta/Al_2O_3/Ta electrodes before (◇) and after (■) molecular attachment.

Molecules on Photolithography-Liftoff-Produced Molecular Electrodes. Instability associated with ion-milled MEME prompted us to investigate whether a simple liftoff process on cross junctions could produce robust molecular electrodes of similar design. In addition to stability, there is a significant advantage of a simple, inexpensive, and scaleable process for device integration. Samples with Si/SiO_2 (100 nm), Co (8 nm), NiFe (2 nm), Al_2O_3 (2 nm), and NiFe (10 nm) film thicknesses (bottom to top) were prepared by the photolithography method of Figure 2, Scheme B. Transport studies of the photolithography-liftoff-produced MEME sample before and after molecule attachment, Figure 5b, showed similar, but more pronounced, effects on transport as seen with the ion-milling-produced MEME sample. For the tunnel junction produced by the photolithography and liftoff process, and whose data are presented in Figure 5b, current at 100 mV before and after molecule attachment was 3.5×10^{-7} and 5×10^{-6} A, respectively. These results strongly suggest that MEME samples, produced via photolithography-liftoff-based approaches, contain a sharp perpendicular side plane that is necessary for attachment of **1**.

Another key merit of the MEME electrode design strategy is the ability to incorporate a variety of metals that function as electrodes. Tantalum, a relatively unexplored metal electrode in the field of molecular electronics, was utilized to construct photolithographically defined cross-junction devices, in an attempt to improve the quality of the insulator layer of the electrodes. Due to the ease of oxidation, Ta can have improved "wetting" of Al_2O_3, thus producing robust tunnel barriers.[21] Photolithography-liftoff-produced MEME samples with (bottom to top) Si/SiO_2 (100 nm), Ta (12 nm), Al_2O_3 (∼2.5 nm), and Ta (12 nm) configurations were prepared, and the transport behavior of assembled devices was measured in the absence and presence of **1** (Figure 6). Relative to bare electrodes, molecular attachment affords a ca. 28-fold increase in the measurable current, due to higher insulator film quality in the Ta system. The reported MEME current before and after molecule attachment at 100 mV was 6.4×10^{-10} and 1.8×10^{-8} A, respectively. Further current enhancement relative to background current is anticipated, assuming that the planar

(21) Dorneles, L. S.; Sommer, R. L.; Schelp, L. F. *J. Appl. Phys.* **2002**, *91*, 7971−7973.

tunnel junction area can be reduced to thinner line widths, from 5 μm to 0.045 μm that is currently possible via conventional photolithographic approaches.

Molecular current is defined as the total current minus the current found for bare electrodes at any given bias. Given that the electrode junctions are ca. 5 μm long and are spaced 1 nm apart and that the average molecular width of **1** is ca. 2 nm, a close-packed array of approximately 10,000 molecules can covalently attach to the exposed lengths (two sides) of the electrodes. At 50 mV applied bias, the average current per molecule was estimated to be 0.16 ($\pm$0.13) nA per molecule, for 48 photolithography-liftoff-produced MEME samples, utilizing Ni and NiFe metal electrodes. The experimental molecular current was of the same order but varied significantly in magnitude between samples. On a linear scale, where the median is near a standard deviation from zero, the larger values of data can skew the standard deviation. So another useful way to state the observed current per molecule is log[current (A)] which is -10.01 ± 0.52. We tentatively propose that the variation in calculated current per molecule values between samples arises from variations in tunnel junction pattern edge quality. However, these edge variations are extremely small, when compared to the current per molecule observed, and are much smaller than values reported for most molecular electrode devices.[22,23]

Control Experiments. A series of control experiments [(i) contact angle study to ensure metal/molecule surface reaction, (ii) effect of electrochemical treatment of electrodes in neat solutions and subsequent rinsing, (iii) reversible molecule attachment and corresponding change in current, (iv) attachment of short-length *n*-butylthioacetate and 20-carbon-long alkane dithiol chain, and (v) increasing alumina thickness beyond the length of molecular bridge] were performed to demonstrate that the observed increases in current were due to the desired surface molecules spanning across the MEME electrode rather than experimental artifacts resulting in uncontrolled surface conduction.

To probe the presence of surface-bound molecules on NiFe electrodes contact angle measurements (using water) were preformed on bare and **1**-modified NiFe films.[24] For unpatterned thin films of NiFe, electrochemical treatment with CH_2Cl_2 solutions of **1** afforded contact angle changes from 11° to 54°; as a control experiment, bare NiFe thin films were rinsed with CH_2Cl_2 and 2-propanol under identical experimental conditions, affording a modest increase in contact angles (to 34°), presumably due to alcohol and/or hydroxyl substitution. This highly water-insoluble molecule under our experimental conditions functionalized the NiFe surfaces in a manner consistent with that in previous in-depth studies using XPS.[23]

In a second series of experiments, the MEME samples were subjected to CH_2Cl_2, cycled potentiometrically in the absence of **1**, and rinsed as previously described; *no increase in current was observed*, suggesting that **1** is necessary for charge transport in MEME tunnel junctions and electrochemistry performed for molecule attachment does not change the conductivity of the exposed edge tunnel junction. Immersion of the MEMEs in a dichloromethane solution of **1** without performing the electrochemical step did not affect transport properties of the exposed edge tunnel junctions. Distilled dichloromethane, where trace HCl was still present, acted to controllably etch any surface oxides for a clean metallic surface for thiol functionalization.

The most important control experiment was to show the reversibility of molecular attachment across the electrode and hence show that there was not any serendipitous breakdown of the electrode at the time of molecular attachment. A photolithography-liftoff-fabricated MEME sample with Ni bottom and Au top metal electrodes(Ni (10 nm)/Al_2O_3 (2 nm)/Au (10 nm) configuration) had bond enthalpies for Ni−S of 344 kJ/mol and for Au−S of 125 kJ/mol.[25,26] Since the Au−S bond is readily reversible, it was possible to remove the thiol linkage by mass-action/exchange in a thiol-alkane solution, to form a self-assembled monolayer of electrically insulating alkanes on the top Au metal electrode. We postulate that this should disconnect the molecule from the top electrode and reduce current to the background level of original electrode current without the molecules. Shown in Figure 7a is the $I-V$ measurement of the bare electrode, after attachment of the conducting molecule, and following exchange of the thiol group of the alkyl tether of **1** with the thiol group of 1-dodecanethiol after exposure to a 5 mmol solution of 1-dodecanethiol in ethanol for 45 min (after first Au−S(1) exchange). The current rose with molecular attachment treatment (as seen before) and then returned to the original bare electrode current level after the exchange reaction with the top Au electrode. The cycle was repeated again (Figure 7b), and the same reversible behavior was exhibited, demonstrating that increase in current is due to the molecular attachment across the insulator, not due to the serendipitous breakdown of the insulator. A slight increase in current for the second functional attachment was expected for an increased number of molecules due to the second molecular attachment treatment. The same displacement experiment performed on Ni/Al_2O_3/Ni electrodes did not show the effect of the thiol-exchange reaction (i.e., a reduction in current) upon exposure to thiol-alkane solution (Figure 7c). This is consistent with the thiol−Ni bond enthalpy being much stronger than that of Au, and hence not reversible. This series of experiments also demonstrated that the molecular current was not due to uncontrolled physisorption of molecules at the electrode surface. The use of a top Au electrode offers chemical sensing possibilities since the top lead of a tethered conducting molecule may be reversibly disconnected by coordination to a sterically bulky analyte molecule.

In our fourth control experiment we probed the effect of a molecule with a single thioacetate end group that was unable to bridge the insulating film of the exposed edge tunnel junction. For this study 2 mM *n*-butane thioacetate solution in dichloromethane was used to electrochemically attach the short molecules on NiFe [12 nm]/Al_2O_3 [2.0 nm]/ NiFe [12 nm] tunnel junctions. On 25 such tunnel junctions, a small increase of 17 $\pm$ 16% over bare tunnel junction current due to *n*-butylthioacetate was observed, indicating that uncontrolled surface chemistry is not responsible for conduction increase. For comparison, bridging molecule **1** produced current increases as high as 5000% over bare tunnel junction current on the samples prepared

(22) Akkerman, H. B.; Blom, P. W. M.; de Leeuw, D. M.; de Boer, B. *Nature* **2006**, *441*, 69−72.
(23) Jeon, D. M.; Park, J. W.; Lee, D. H.; Yoon, S. Y.; Yoon, D. H.; Suh, S. J. *J. Magn. Magn. Mater.* **2004**, *272−276*, 1956−1958.
(24) Mekhalif, Z.; Laffineur, F.; Couturier, N.; Delhalle, J. *Langmuir* **2003**, *19* (3), 637−645.
(25) Lide, D. R. *CRC Handbook of Chemistry and Physics.*
(26) Ruan, C. M.; Bayer, T.; Meth, S.; Sukenik, C. N. *Thin Solid Films* **2002**, *419*, 95−104.

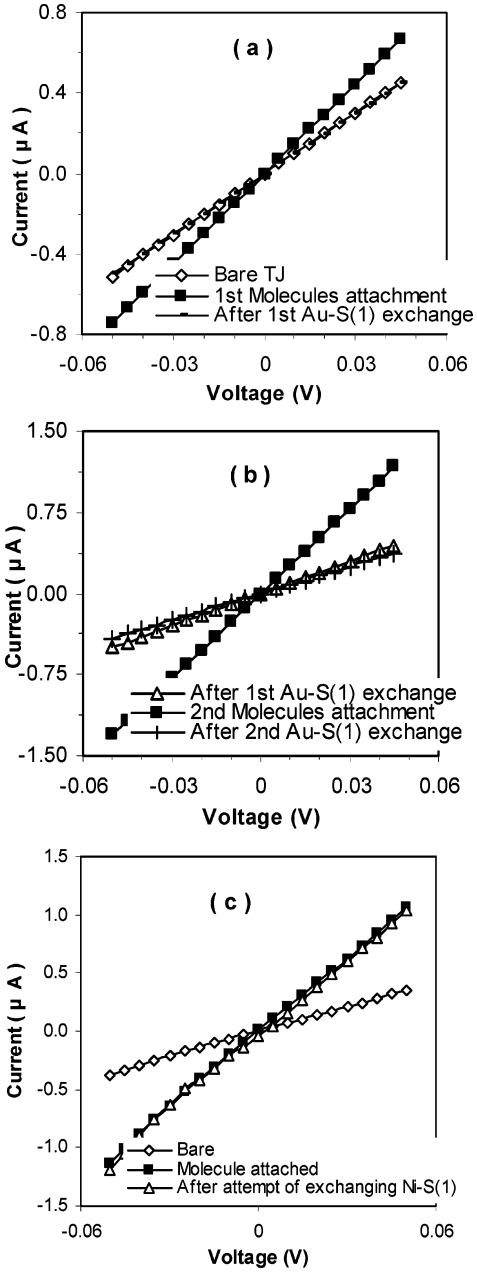

Figure 7. Reversible displacement of alkyl tether of **1** on top Au electrode is observed upon treatment with thiol-exchange reaction. Current−voltage characteristics of a Ni/Al_2O_3/Au multilayer edge containing **1** and upon treatment with 5 mM 1-dodecanethiol. (a) Bare electrode before (◇) after (■) molecular attachment of **1** and after thiol exchange of tether from top electrode with the thiol group of 1-dodecanethiol (■). (b) Repeated experiment using the same sample: (Δ) after first thiol exchange (last step of Figure 7a), (■) **1** addition, and (+) after second thiol-exchange reaction at top Au electrode. (c) Ni/Al_2O_3/Ni molecular junction was not affected by thiol-exchange reaction showing reversibility of only the top Au electrode (7a,b). Bare electrode before (◇) and after (■) molecular attachment of **1** and after the attempt to exchange Ni−thiol bond (△) with 1-dodecanethiol solution.

under the same conditions. This experiment clearly suggested that just the formation of the metal−thiol bond on the surface is not sufficient to affect the conduction process of exposed edge tunnel junction (MEME). We have also attached a 20-carbon long alkane with thioacetate groups at each end to span the NiFe/Al_2O_3/ NiFe samples. A 2 mM solution of this molecule in dichloromethane was used in the process. Modest

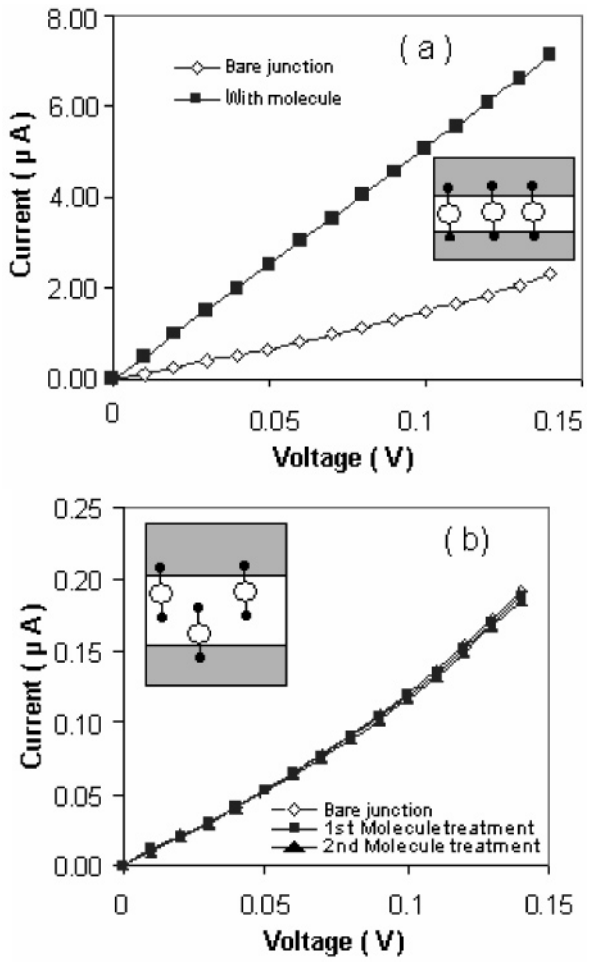

Figure 8. Molecule with propylthioacetate tether (∼2.4 nm long) on NiFe/Al_2O_3/NiFe tunnel junction produced by Scheme B, Figure 2. (a) Molecule attachment on ∼2-nm thick tunnel barrier (shorter than molecule length), (b) attachment on a ∼3-nm thick tunnel barrier (thicker than molecule length).

current increases of 84 ± 57% (20 samples) over bare MEME current were observed, consistent with the relatively poor conduction through an alkane tether bridging the insulator gap.

In the last control experiment we saw that current increase on the exposed edge of the tunnel junction was only possible when the molecule was long enough to span the oxide barrier. Molecule **1** was modified to have short *hexyl* thioacetate tethers, resulting in an overall length of ∼2.4 nm. For this study two MEME electrodes (NiFe/Al_2O_3/NiFe), the first with ∼2 nm and the second with ∼3 nm Al_2O_3 barrier thicknesses, were used. The exposed edge tunnel junction with 2-nm thick Al_2O_3 (tunnel barrier thickness < molecule length) showed a clear increase in current (Figure 8a) but the tunnel junction with 3-nm thick Al_2O_3 (tunnel barrier thickness > molecule length) showed no increase in current Figure 8b. This is further confirmation that uncontrolled surface chemistry does not provide a dominant current path.

Analysis of Electron Transport via Simmons Tunneling Model. The electron-transport properties of various MEME samples, with different insulator thicknesses and in the presence and absence of **1**, were analyzed via the Simmons tunnel current model. By fitting observed current density (j)-voltage (V) data to the Simmons model within a medium voltage range (V <

φ_B/e) as shown in eq 1:[27]

$$j = \left(\frac{e}{4\pi^2\bar{h}d^2}\right)\left\{\left(\varphi_B - \frac{eV}{2}\right)\exp\left[-\frac{2(2m)^{1/2}}{\bar{h}}\alpha\left(\varphi_B - \frac{eV}{2}\right)^{1/2}d\right] - \left(\varphi_B + \frac{eV}{2}\right)\exp\left[-\frac{2(2m)^{1/2}}{\bar{h}}\alpha\left(\varphi_B + \frac{eV}{2}\right)^{1/2}d\right]\right\} \quad (1)$$

where m is electron mass, d is barrier thickness, φ_B is barrier height, V is applied bias, and α is a unitless adjustable parameter, that allows for deviations from a simple rectangular barrier and effective mass of the electron.[28] Via eq 1, (setting $\alpha = 1$) we are able to fit the values of both barrier height and barrier thickness before and after molecule attachment for various MEME samples.

To validate the Simmons model in our system, a comparison was made between the calculated thickness of alumina (present in a bare MEME tunnel junction) from the Simmons model and the physical thickness of a pattern of alumina (grown under identical conditions) as measured by AFM. Calculated and measured thicknesses of alumina were in agreement within experimental uncertainty (2 Å). Moreover, the calculated values of barrier height of alumina used in MEME samples closely matched barrier height values found for alumina films in other studies of alumina tunnel junctions.[23] It is important to note that the Simmons model, originally established for the simple tunnel barrier between two nonmagnetic metal electrodes, can be used to study the rate-limiting steps in complex systems such as magnetic tunnel junctions and spin filters.[29]

For modeling purposes, molecular current (at any bias) is defined as the total molecular electrode current after molecule attachment *minus* the current of the bare electrode. The bare tunnel junction area is 25 μm^2, and an effective tunnel area for molecular current is calculated in the following manner. Via X-ray structural studies, **1** is approximately 1 nm wide (Fe−Ni edge) and attaches to the electrode edge in a close-packed arrangement along a 10-μm insulator line as shown in Figure 1b. Considering that the alkane tethers also occupy space and the cluster core is insulated from its surroundings by the coordinated ligands, the most likely conduction pathway is likely to be through the S(alkyl) chain. As a result, charge enters and leaves the cluster core and tunnels through the alkyl chains, giving a total molecular tunnel area of 1×10^{-10} cm^2 (=10 $\mu m \times 1$ nm). Having obtained the experimental current density, molecular barrier height and barrier thickness were calculated using the Simmons model as shown in eq 1. The fitting of eq 1 to observed data converged to unique solutions with an uncertainty of 0.1 eV in barrier height and 1 Å in barrier thickness.

Effective barrier heights for the molecular transport component of electrodes functionalized by **1** were calculated for a series of MEME samples with magnetic (NiFe) and nonmagnetic metal (Ta) electrodes. Generally, molecular barrier height values were significantly less than those of bare MEME samples with tunneling only through the alumina layer. The molecular barrier height values had significant variation with magnetic metal electrodes (NiFe) (0.67 ± 0.3 eV); however, relatively less variation was seen with the nonmagnetic Ta metal electrodes (0.74 ± 0.16 eV), for the data shown in graphs, as seen in Figure 9a. The scatter in current is presumably linked to spin effects of the molecule coupled to magnetic leads and is currently being studied. In Figure 7b, the barrier thickness (1.27 ± 0.27 nm) calculated from the molecular $I-V$ data is consistent with the expected length of an insulating decyl tether. However, the overall molecular dimensions (via X-ray) are estimated to be ca. 3 nm overall, due to 2 decyl tethers (ca. 1.2 nm length) and a $\{Fe^{III}_4Ni^{II}_4(CN)_{12}\}$ core (ca. 1 nm). The anticipated energy level diagram of the MEME before and after attachment of **1**, which resembles the energy diagram expected for a double barrier tunnel junction,[29] is shown in Figure 10. In the case of the 20-carbon-long alkane dithiol (control experiment iv) the idealized band diagram in Figure 10 is similar to the bare MEME case with reduced barrier height. A key merit to this metal-cluster geometry is to force conduction through a reduced tunnel barrier thickness into a well-defined molecule state *as the limiting current step*. By tailoring the core molecular state through synthesis, true molecule-based electronic devices can be realized.

Support for molecule-mediated charge transport being the dominant conduction pathway was obtained via temperature-

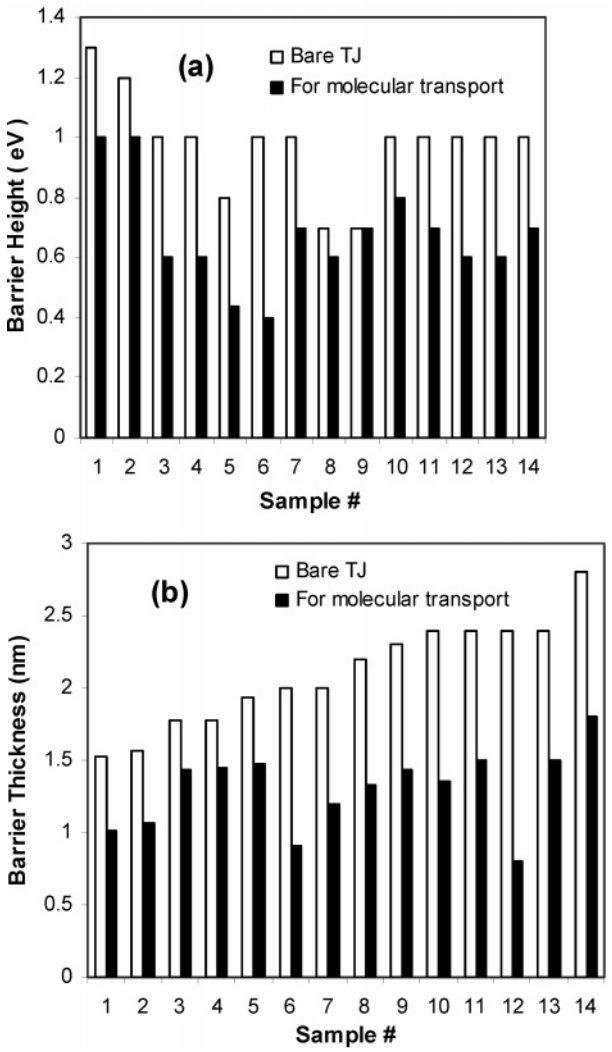

Figure 9. Barrier height (a) and barrier thickness (b) for photolithography-liftoff-produced samples with NiFe magnetic metal electrodes (samples 1−9) and nonmagnetic Ta metal electrodes (samples 9−14).

(27) Simmons, J. G. *J. Appl. Phys.* **1963**, *34*, 1793−&.
(28) Wang, W. Y.; Lee, T.; Reed, M. A. *Phys. Rev., B* **2003**, *68*, 3.
(29) Moodera, J. S.; Hao, X.; Gibson, G. A.; Meservey, R. *Phys. Rev. Lett.* **1988**, *61*, 637−640.
(30) Ricco, B.; Azbel, M. Y. *Phys. Rev., B* **1984**, *29*, 1970−1981.

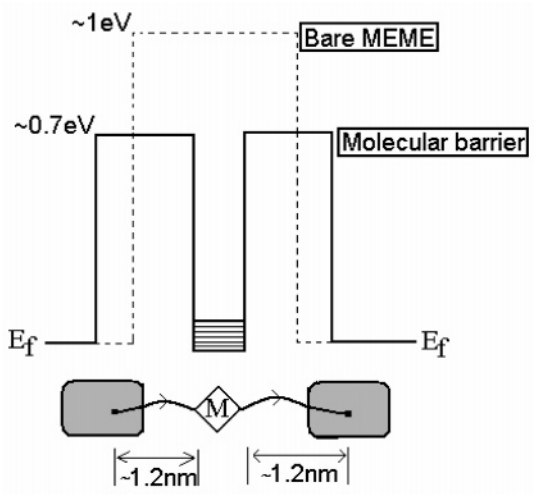

Figure 10. Idealized band diagram of tunnel junction before (···) and after (—) attachment of **1**. E_f Fermi energy levels of metal electrode, where ~1 eV is the barrier height of the bare tunnel junction, ~0.7 eV is the barrier height of the insulating alkane tether.

dependent transport studies. These were obtained between 25 and 100 °C, using the photolithography-liftoff-produced MEME sample [Ta (10 nm)/Al_2O_3 (2.5 nm)/Ta (10 nm)]. Temperature effects are possible only when molecular excitation, essentially coupled to molecular transport, can be produced at the center of the molecule. The tunneling transport mechanism through the alumina insulator and alkane tether is essentially temperature independent.[28] Upon heating, the sample current increases, corresponding to a thermally activated transport process, with a ca. 0.30 (±0.02) eV activation energy barrier. This estimated activation energy barrier is consistent with activation energies expected for conformational changes[31] and calculated transport activation energies reported for other molecules.[32] The thermal barrier is also significantly less than the full barrier height observed by the tunnel current model. The data also suggest that the transport mechanism is more complicated than a simple elastic tunneling process (thermally assisted tunneling) but are consistent with the idealized molecular geometry on the electrode surface proposed. Our molecule has two tunnel barriers (due to alkane tethers) separated by an organometallic cube with conjugated bonds, which provide density of states closer to the metal electrodes Fermi level.[33] For small area double tunnel barrier systems it is reported that both elastic and inelastic processes contribute to the current and direct tunneling is more prominent toward a lower temperature range.,[34] In the transport study of several single-molecule magnets, transition between pure quantum tunneling (temperature independent) to thermally assisted tunneling (temperature dependent) was observed.[35] In this molecular geometry the current rate-limiting step would be tunneling into or out of the molecular center through the alkane tether, and this is the basis for our rationale in the application of the Simmons model to this rate-limiting step. Due to adverse thermal stresses on MEME stability we are currently unable to perform cryogenic transport studies. However, the

Table 1. Barrier Thickness and Height Estimated via Simmons Tunnel Current Model Fits of Conduction through Assembled Ta/Al_2O_3/Ta Multilayer Edge Molecular Electrodes

	barrier thickness (nm)	barrier height (eV)
bare electrode tunnel barrier	2.48 (±0.18)	0.94 (±0.13)
molecular tunnel barrier	1.30 (±0.29)	0.74 (±0.16)

cutoff temperature for several molecular systems is close to room temperature; e.g., for terphenyl and nitroazobenzene molecules the thermally activated conduction process freezes out near 10 °C.[32] Temperature studies of these molecular junctions are ongoing and largely limited by the control of film stresses during the growth process.

Additional support for a qualitative tunneling conduction model can be inferred from the calculated value of the tunneling decay coefficient (β).[36] An exponential decrease in current ($I \propto \exp(-\beta d)$) with alkane length (d) was commonly measured. Here β was extracted (for only one alkane length) from our calculated barrier heights and thickness from the Simmons model for nonmagnetic MEME samples whose barrier properties are given in Table 1. We experimentally observed a β of 0.88 (0.10) $Å^{-1}$, which was remarkably close to the observed value of $\beta = 0.85$ $Å^{-1}$ for an alkane tether of similar length as seen in STM studies of individual molecules and from self-assembled monolayers of thiol-alkanes.[28,36]

A qualitative transport consistent with our experimental observations is: [1] tunneling of electrons from the left (or right) metal electrode to the organometallic cube present in the center of molecule, [2] quick charge transport through the organometallic cube, and [3] tunneling from the organometallic cube toward the right (or left) metal electrode. The expression for the total time of charge transfer (t_{Total}) through the molecular junction is given in eq 2:

$$t_{Total} = t_1 + t_2 + t_3 \quad (2)$$

t_1, t_2, and t_3 are the inverses of the charge transport rates through the first alkane tether, the organometallic cube, and the second alkane tether, respectively. The tunneling rate is expected to be much slower than transport rate through conjugated bonds enriched organometallic cube of **1**,[33] which implies that $t_2 \ll t_1 \approx t_3$. This would result in the overall conduction to be rate limited by the tunneling rate through the alkane tether either to or from the molecule cluster core.

Conclusions

By using the exposed face at the edge of a multilayer thin film pattern, an electrode with nanometer-scale distance between metal leads was reliably formed. Importantly, the critical dimension was controlled to molecular lengths with angstrom-scale precision using conventional deposition processes. Since the pattern can be defined by photolithography, the economical large-scale integration of molecular electrodes can be readily achieved, using the described approach. In our study, molecular electrodes with insulator thicknesses ranging from 1.5 to 2.5 nm were studied. The cross-junction array can utilize recently developed two-terminal logic designs,[10] or alternatively, the edge

(31) Di Ventra, M.; Pantelides, S. T.; Lang, N. D. *Appl. Phys. Lett.* **2000**, *76*, 3448−3450.
(32) Anariba, F.; McCreery, R. L. *J. Phys. Chem. B* **2002**, *106*, 10355−10362.
(33) Piccinin, S.; Selloni, A.; Scandolo, S.; Car, R.; Scoles, G. *J. Chem. Phys.* **2003**, *119*, 6729−6735.
(34) Averin, D. V.; Nazarov, Y. V. *Phys. Rev. Lett.* **1990**, *65*, 2446−2449.
(35) Park, C. S. *J. Magn. Magn. Mater.* **2003**, *267*, 281−288.
(36) Cui, X. D.; Zarate, X.; Tomfohr, J.; Sankey, O. F.; Primak, A.; Moore, A. L.; Moore, T. A.; Gust, D.; Harris, G.; Lindsay, S. M. *Nanotechnology* **2002**, *13*, 5−14.

geometry can be incorporated into more conventional, arbitrarily addressed junctions. This edge geometry does not readily incorporate an electrostatic gate at close proximity; however, electrostatic switching of molecules typically requires extremely high electric fields (~100 MeV/cm),[31] that far exceed the breakdown point of known dielectrics. This two-terminal device architecture approach has two major merits other than ease of integration. First, a wide range of materials can be introduced on alternate sides of an insulating barrier, including magnetic materials, allowing for the possibility of current modulation via the spin state of the bridging metal cluster. Second, all conductive molecules reside on the exposed surface allowing for strong selective chemical interactions with analyte molecules. In principle, a bound analyte molecule can change the conformation of the conduction molecule or force the reversible removal of a tether from a top gold contact, which may lead to the design of a reversible sensing device. Furthermore, the planar electrode geometry also provides for further conformational constraint of the molecule on the surface, which may be an important consideration in improving the molecular conduction process. The relative simplicity of this electrode geometry allows for a significant improvement in the ability to study molecular conduction and may finally enable molecules to be incorporated into large-scale device architectures.

Acknowledgment. We thank Bing Hu for the SEM study of cross junctions. Support was generously provided by the Air Force Office of Scientific Research (DEPSCoR) under agreement number F49620-02-1-0225, the Kentucky Science and Engineering Foundation (KSEF-621-RDE-006 and KSEF-992-RDE-008), the American Chemical Society Petroleum Research Fund (PRF 38388-G3), and the University of Kentucky Research Support Grant and Major Research Project Programs for partial support of this research.

Supporting Information Available: Additional data and analysis for the fit of the Simmons tunnel model to observed experimental data. This material is available free of charge via the Internet at http://pubs.acs.org.

JA065789D